Journal of Structural Geology 106 (2018) 54–69

Contents lists available at ScienceDirect

Journal of Structural Geology

journal homepage: www.elsevier.com/locate/jsg

# 3D mechanical stratigraphy of a deformed multi-layer: Linking sedimentary architecture and strain partitioning

Adam J. Cawood*, Clare E. Bond

*Department of Geology and Petroleum Geology, School of Geosciences, University of Aberdeen, Meston Building, Kings College, Aberdeen, AB24 3UE, UK*

ARTICLE INFO

*Keywords:*
3D mechanical stratigraphy
Strain partitioning
Virtual outcrop
Multi-layer

ABSTRACT

Stratigraphic influence on structural style and strain distribution in deformed sedimentary sequences is well established, in models of 2D mechanical stratigraphy. In this study we attempt to refine existing models of stratigraphic-structure interaction by examining outcrop scale 3D variations in sedimentary architecture and the effects on subsequent deformation. At Monkstone Point, Pembrokeshire, SW Wales, digital mapping and virtual scanline data from a high resolution virtual outcrop have been combined with field observations, sedimentary logs and thin section analysis. Results show that significant variation in strain partitioning is controlled by changes, at a scale of tens of metres, in sedimentary architecture within Upper Carboniferous fluvio-deltaic deposits. Coupled vs uncoupled deformation of the sequence is defined by the composition and lateral continuity of mechanical units and unit interfaces. Where the sedimentary sequence is characterized by gradational changes in composition and grain size, we find that deformation structures are best characterized by patterns of distributed strain. In contrast, distinct compositional changes vertically and in laterally equivalent deposits results in highly partitioned deformation and strain. The mechanical stratigraphy of the study area is inherently 3D in nature, due to lateral and vertical compositional variability. Consideration should be given to 3D variations in mechanical stratigraphy, such as those outlined here, when predicting subsurface deformation in multi-layers.

## 1. Introduction

Understanding how deformation processes are impacted by the inherent compositional heterogeneity of the rock volume being deformed is a key question in structural geology. The complex interplay of stratigraphic heterogeneity and structural mechanisms is well documented at multiple scales of observation and in a range of tectonic settings. Studies have addressed this interaction at thin section (e.g. Hooker et al., 2013), outcrop (e.g. Lloyd and Chinnery, 2002; Butler and McCaffrey, 2004; Roche et al., 2012) and regional (e.g. Woodward and Rutherford, 1989; Pfiffner, 1993; Mitra, 2003; Ferrill and Morris, 2008) scales, and have focussed on extensional (e.g. Morris et al., 2009; Ferrill et al., 2007, 2016) and contractional (e.g. Couzens and Wiltschko, 1996; Farzipour-Saein et al., 2009) tectonic regimes, at a range of temperatures and depths (e.g. Amilibia et al., 2008; Druguet et al., 2009; Poblet and Lisle, 2011). The concept of mechanical stratigraphy, defined as the mechanical properties of units, their relative thicknesses, unit spacing and the nature of unit boundaries, has developed, from such studies, in an attempt to improve understanding of deformation patterns in multi-layers.

Mechanical stratigraphy, or the differences in mechanical properties through a given sequence, has long been known to influence the localisation of strain in contractional settings (Willis, 1893). This concept has been used to explain a range of structural features and patterns, and has been found to influence style of folding (e.g. Couples and Lewis, 1999; Bastida et al., 2007), disharmony in folds (e.g. Currie et al., 1962; Pfiffner, 1993; Mitra, 2003), the presence of thrust and fold detachments in mechanically weak layers (e.g. Couzens and Wiltschko, 1996; Tavani et al., 2008; Vergés et al., 2011), partitioned vs distributed strain (e.g. Couples and Lewis, 1999; Fischer and Jackson, 1999; Van Noorden et al., 2007), and the evolution of mechanical stratigraphy through progressive deformation (e.g. Hayes and Hanks, 2008). Much emphasis has been placed on the role of mechanical stratigraphy in influencing fracture distributions (e.g. Ladeira and Price, 1981; Corbett et al., 1987; Laubach et al., 2009), and the importance of considering stratigraphic heterogeneity in conjunction with structural attributes when making predictions of fracture distributions (Zahm and Hennings, 2009). The concept of mechanical stratigraphy has thus led to a refinement of mechanical models to aid in their predictive ability.

While the concept of mechanical stratigraphy to explain and predict structural behaviour is a powerful tool, these models are generally applied to continuous sedimentary sequences based on 2D sections

* Corresponding author.
*E-mail address:* adam.cawood@abdn.ac.uk (A.J. Cawood).

https://doi.org/10.1016/j.jsg.2017.11.011
Received 11 September 2017; Received in revised form 14 November 2017; Accepted 19 November 2017
Available online 24 November 2017

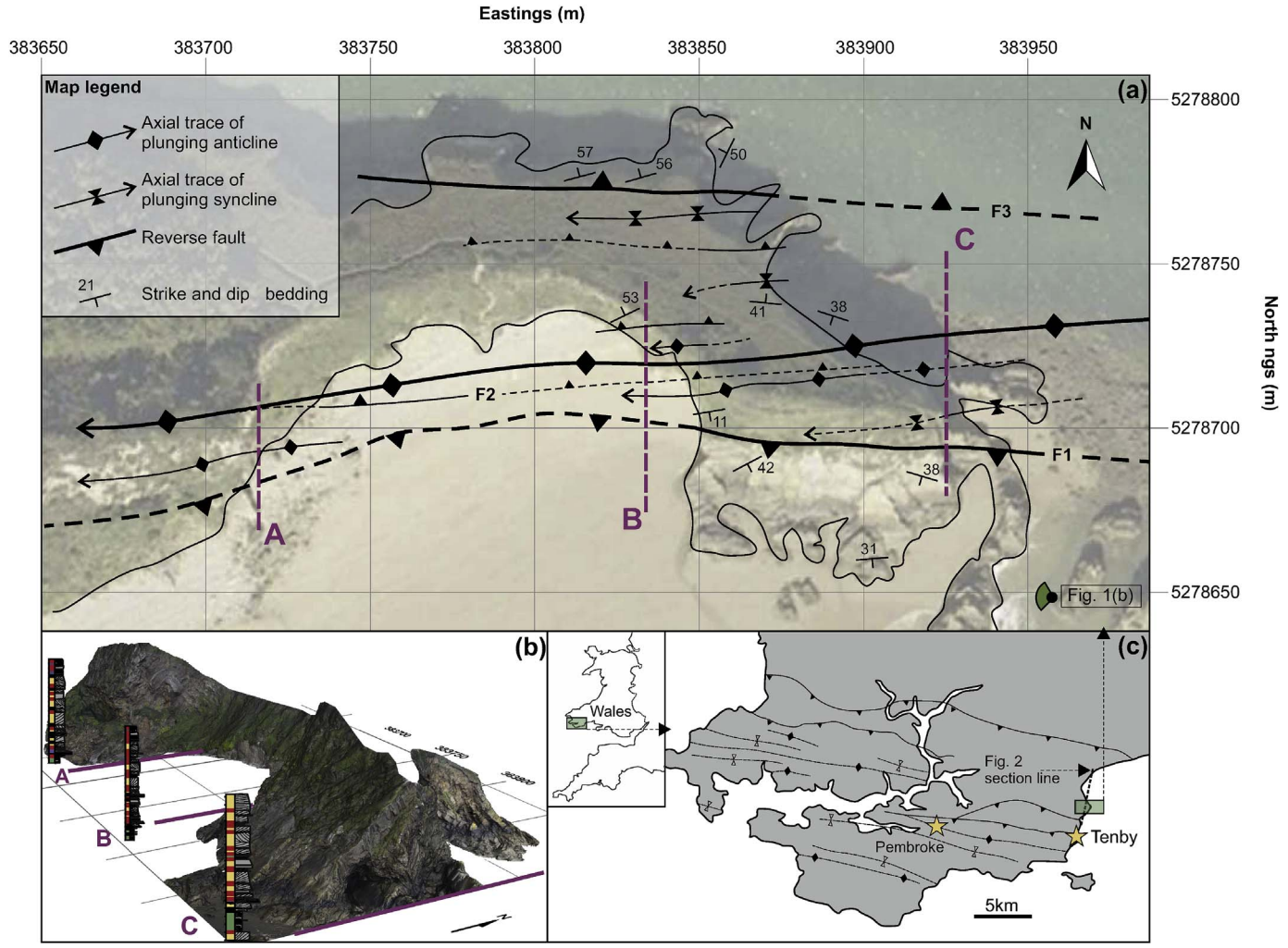


**Fig. 1.** Monkstone Point, Pembrokeshire. (a) Structural map of study area from in-field measurements, observations and virtual outcrop analysis. Purple lines mark cross-section locations (Fig. 8); green semi-circle denotes approximate camera location and field-of-view for Fig. 1b. Map coordinates: UTM Zone 31N. (b) Perspective view of Monkstone Point virtual outcrop, with locations of logs (see Fig. 4 for larger scale logs) and cross-section lines (see Fig. 8). (c) Summary structural map of Pembrokeshire (after Coward and Smallwood, 1984). (For interpretation of the references to colour in this figure legend, the reader is referred to the web version of this article.)

through the stratigraphy. Mechanical layer and interface properties of rock units are commonly greatly simplified and presumed to be internally homogenous and laterally continuous. Only rarely is the presence of heterogeneities internal to units (e.g. Zahm and Hennings, 2009) or the superposition of structure on outcrop-scale sedimentary features (e.g. Hancock et al., 1982; Tringham, 1985; Nicol et al., 2002) acknowledged when considering stratigraphic-structure interactions, albeit in 2D. Some studies have addressed this interaction in 3D, using seismic data, e.g. Mansfield and Cartwright (1996) who describe the development of multiple thrust faults in different sedimentary layers, that later link into single through-going thrusts. Kristensen et al. (2008) and Roche et al. (2012) focus on, macro-mesoscale scale extensional faults highlighting complexities in fault evolution, branch patterns and relay development controlled in part by mechanical contrasts in the multi-layer systems studied.

This study assesses the effects of 3D depositional heterogeneity (stratigraphic architecture) on strain partitioning at an outcrop scale. Our example is from the contractional setting of Monkstone Point in Pembrokeshire, SW Wales (Fig. 1), which exposes a layered sequence of deformed clastic sediments. A genetic-link is predicted between the 3D stratigraphic architecture and the degree of strain partitioning within this multi-layer succession. Using sedimentary/structural logging, Structure from Motion photogrammetry, compositional analysis of samples and structural measurements we provide a detail analysis of the outcrop and document the extent and localisation of partitioned strain during contractional deformation. This strain partitioning manifests itself as different structural styles within and across layers in the outcrop. We discuss the findings of our work in the context of understanding 3D mechanical stratigraphy in non-planar multi-layer sedimentary successions, mechanical stratigraphy in contractional settings, and the consequent implications for subsurface prediction of structures.

## 2. Geological setting

Monkstone Point lies within the South Wales Lower Coal Measures Formation (312–313 MA), of the Upper Carboniferous (Westphalian), which is dominated by coal-bearing mudstones and siltstones, with minor sandstones present in the lower part of the succession (Jenkins, 1962; Williams, 1968; George, 1982; Waters et al., 2009). This sequence comprises part of the post-rift stratigraphy of SW Wales, postdating units associated with Silurian and Devonian extension. The South Wales Lower Coal Measures Formation is interpreted as fluvio-deltaic in origin (George, 2008), and is characterized locally by distributary channels, coastal plain and delta slope deposits, and shallow marine sequences (Powell, 1989; George, 2000). Channel bodies within the lower part of the succession are characterized by erosive bases and are commonly cross-bedded. Minor seat-earths, overbank deposits and thin coal beds are distributed throughout the succession, and are often

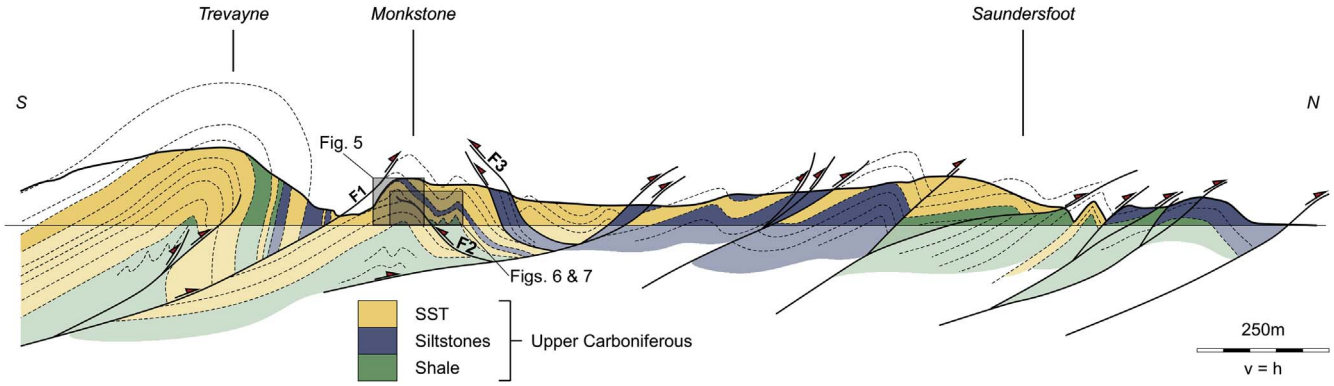


**Fig. 2.** Semi-regional, simplified Trevayne to Saundersfoot cross-section, compiled from Jenkins (1962), Coward and Smallwood (1984), and Smallwood (1985), and data collected for this study. Section line displayed in Fig. 1(c). Shaded boxes correspond to approximate locations of field photographs (Figs. 5–7) and detailed cross sections (Fig. 8 a, b and c). Laterally persistent, bounding thrusts that define geometry of Monkstone anticline named as F1 & F3.

constituents of channel-base lag deposit material (Dixon, 1933). Directly overlying this formation are the South Wales Middle and Upper Coal Measures, deposited in the foreland basin of the advancing Variscan front, which mark the transition from relative tectonic quiescence to a contractional regime (Gayer and Jones, 1989; Powell, 1989) in the Late Carboniferous. It is the deformation resulting from Variscan contraction that is manifest in the sedimentary succession in the study site and is interrogated here.

The northern limit of Variscan deformation in the United Kingdom falls in SW Wales, and dominates the deformation structures in the South Wales Lower Coal Measures Formation. Regionally, the structural trend is WNW – ESE (Fig. 1c), marking NNW-directed Variscan shortening of up to 67% (Frodsham and Gayer, 1997). Vergence of folds and thrust sequences is generally to the NNW (Fig. 2), though deformation is commonly accommodated by back-thrusts with local folds verging to the SSE (Hancock et al., 1982; Gayer and Jones, 1989; Coward and Smallwood, 1984). Inversion of pre-existing Devonian and Dinantian extensional features (Smallwood, 1985; Powell, 1989) influence structural style and the localisation of thrust faults. At outcrop scale, deformation style is highly variable and largely dependent on lithology (Hancock, 1973; Dunne, 1983; Dunne and North, 1990). Relatively incompetent fluvio-deltaic multi-layer sequences of the Upper Carboniferous are generally the most intensely deformed successions in SW Wales, and form some of the best-known fold-thrust outcrop examples in the United Kingdom (De la Beche, 1826; Hancock et al., 1982; Smallwood, 1985; Tringham, 1985; Leveridge and Hartley, 2006).

## 3. Lithostratigraphy

Monkstone Point lies on Pembrokeshire's east coast (Fig. 1c) and is an exposed anticline in the South Wales Lower Coal Measures Formation. Outcrop morphology provides three natural, N-S oriented cliff sections, spaced ~100 m apart (Fig. 1b), allowing examination of lateral and vertical variations in sedimentary facies documented in 65 m of logged section. Natural Gamma Ray (NGR) data was collected for each of the logged sections with a *Radiation Solutions* RS-230 Handheld Radiation Detector. In-field measurements were performed, where possible, on unfractured, continuous rock faces, with the tool held on the rock face for 180 s, providing estimates of %K and ppm values for U & Th. NGR data is presented here as total counts per second (cps). This technique was employed to supplement logging by objectively quantifying changes in composition through the sedimentary succession (Fig. 3). Outcrop NGR measurements provide a quantitative method for assessing heterogeneity in sedimentary successions and thus may improve log-to-log correlation (Aigner et al., 1995). Rock samples provided material for 16 oriented thin sections, from which observations of micro-structure, composition and grain size distributions were made. 38 field samples were further processed and analysed for bulk composition by X-ray fluorescence (XRF), using an *Olympus* DELTA handheld XRF analyser. As with the NGR, this data was used to supplement field data for log-to-log correlation. Notwithstanding the variability in sedimentary architecture logged across the outcrop, the five units described in the sections below were recorded in each of the cliff sections allowing correlation of sedimentary/structural logs (Fig. 4). This contribution is not intended to provide a detailed sedimentological analysis of the study area, but rather to examine how 3D variations in unit compositions impact subsequent deformation. Nonetheless, utilising information from logged sections, field observations and virtual outcrop data, we provide a summary description of units recorded at Monkstone Point.

### 3.1. Mudstone (Unit 1)

A fine-grained mudstone, up to 2.4 m thick, is the base unit of the three logged sections (Figs. 3 and 4). Grain size ranges from ~1-4 μm, and grain composition is dominated by quartz grains, micas and feldspar. High NGR values of 97–178 cps, and correspondingly low Si bulk composition (16–27%) suggest this unit contains a significant amount of ferro-silicates and muddy material, supported by thin section observations (Fig. 3f). Unit 1 was likely deposited in a delta-plain environment, associated with lagoonal or estuarine facies (Bluck and Kelling, 1963). Depositional or erosive contacts of overlying Units 2, 3 and 4 (Fig. 4) suggest this is the stratigraphically oldest unit at Monkstone Point.

### 3.2. Fine interbeds (Unit 2)

Directly above the mudstone (Unit 1) is a laterally discontinuous, chaotic package of mudstones, thin coal horizons with sandstone interbeds (Fig. 3a). This package, 0.2–1.1 m thick, contains numerous intraformational mudstone lag deposits, plant material, and erosive contacts. Variability of grain size (1–15 μm) and NGR counts (94–124 cps), reflect the heterogeneity in this package manifest as rapid transitions in grain size and composition vertically (Fig. 3f). As with Unit 1, Unit 2 probably represents lagoon or estuary deposits, with thin, discontinuous sandstones, coal horizons and terrestrial material representing local, laterally discontinuous variations in depositional environment.

### 3.3. Basal gravel lag (Unit 3)

Unit 3, a gravel lag deposit, incises downwards into Units 1 and 2 and forms the erosive base to the overlying sandstone channel sequence (Units 4 and 5). Clasts within this unit are comprised of quartz and ironstone pebbles mixed with coal fragments, rare plant material and carbonaceous shale, interpreted as locally derived (Bluck and Kelling,

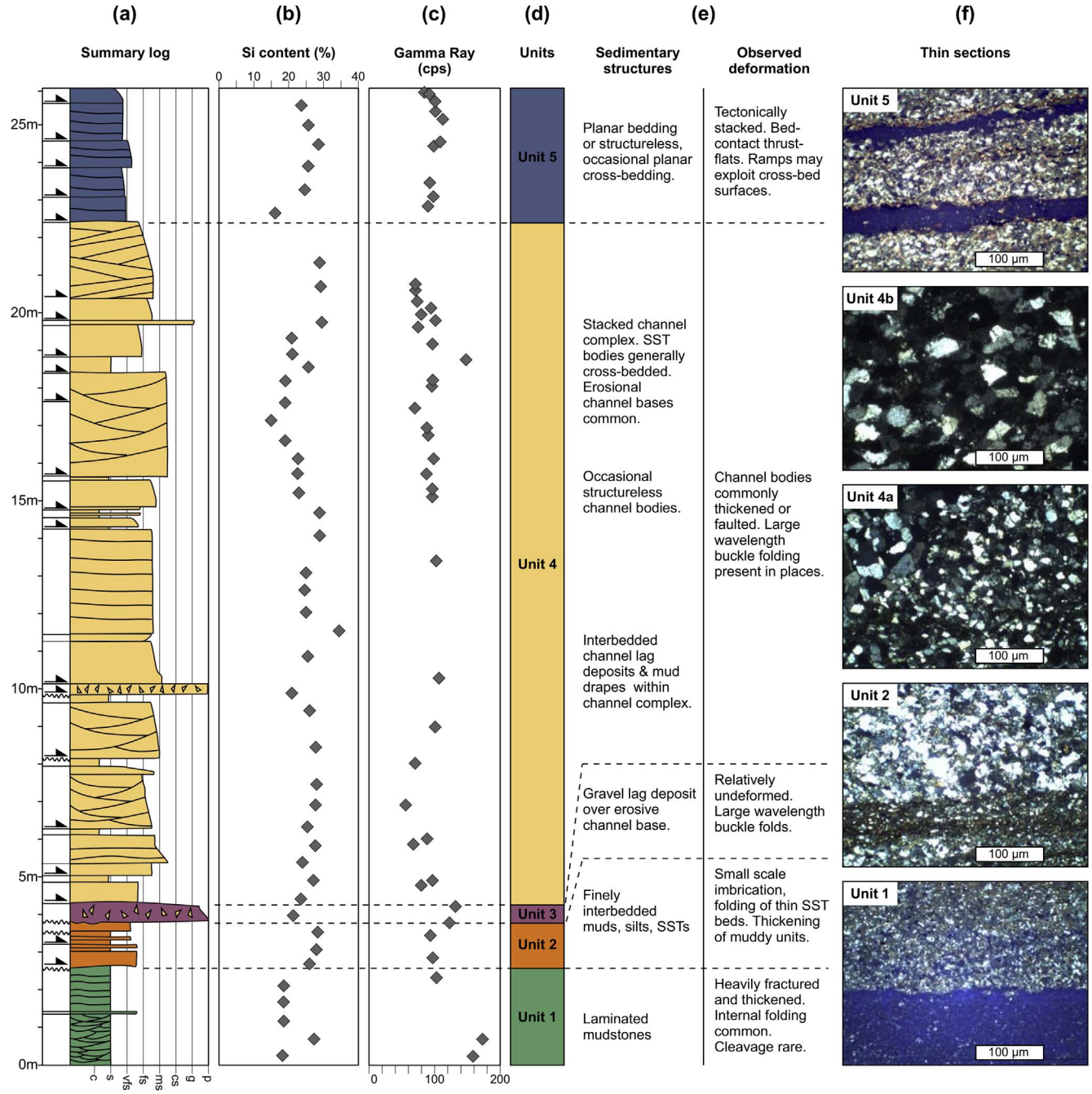


**Fig. 3.** Summary lithostratigraphy for Monkstone Point. (a) Sedimentary log compiled from the integration of 3 separate logged sections (see Fig. 1b for locations). Arrows on far left denote inferred slip horizons; wavy lines mark erosive contacts. Units coloured to correspond with cross-sections. Key for depositional features in Fig. 4. (b) Silica weight percent, from XRF data, compiled from the 3 logged sections, primarily from samples collected at section B (c) Compiled in-field natural gamma ray (NGR) measurements, primarily from samples collected at section B. (d) Assigned units (see section 3). (e) Summary sedimentary/structural features from field and virtual outcrop observations. (f) Thin-sections (cross-polars) from field samples, with assigned units in top left of each image.

1963), with a grain size distribution from silt to pebble sized grains. This unit is laterally continuous across the outcrop (Fig. 4) and has a thickness range of 0.4–2.2 m. The erosive nature of the unit's lower bounding surface and a lack of internal sedimentary structure are suggestive of chaotic, rapid deposition. This gravel lag body records widespread erosion and a marked increase in grain size across the outcrop and thus probably records incision of a major channel in the sedimentary sequence (Miall, 1985).

### 3.4. Sandstone (Unit 4)

This sandstone interval comprises the thickest vertical component (up to 18.3 m) of the sedimentary sequence at Monkstone and lies conformably on, or incises downwards into, Unit 3. In general, this part of the sequence fines upwards, contains an erosive base overlain by finer, siltstone beds and has a composition dominated by quartz grains (> 80%), with a grain size range of 5–25 µm (Fig. 3f). XRF measurements of Si content within this unit (Fig. 3b) were measured from 30 samples (24 of which were sampled in log B). The silica content range (15–34.5%) in Unit 4 reflects compositional variability within this unit. Similarly, Gamma Ray counts, from 27 measurement sites in Unit 4, display a range of values (63–146 cps). NGR and XRF data (Fig. 3b and c), along with field logs (Fig. 4), also record these lateral and vertical variations in the composition of Unit 4. Compositional variation is

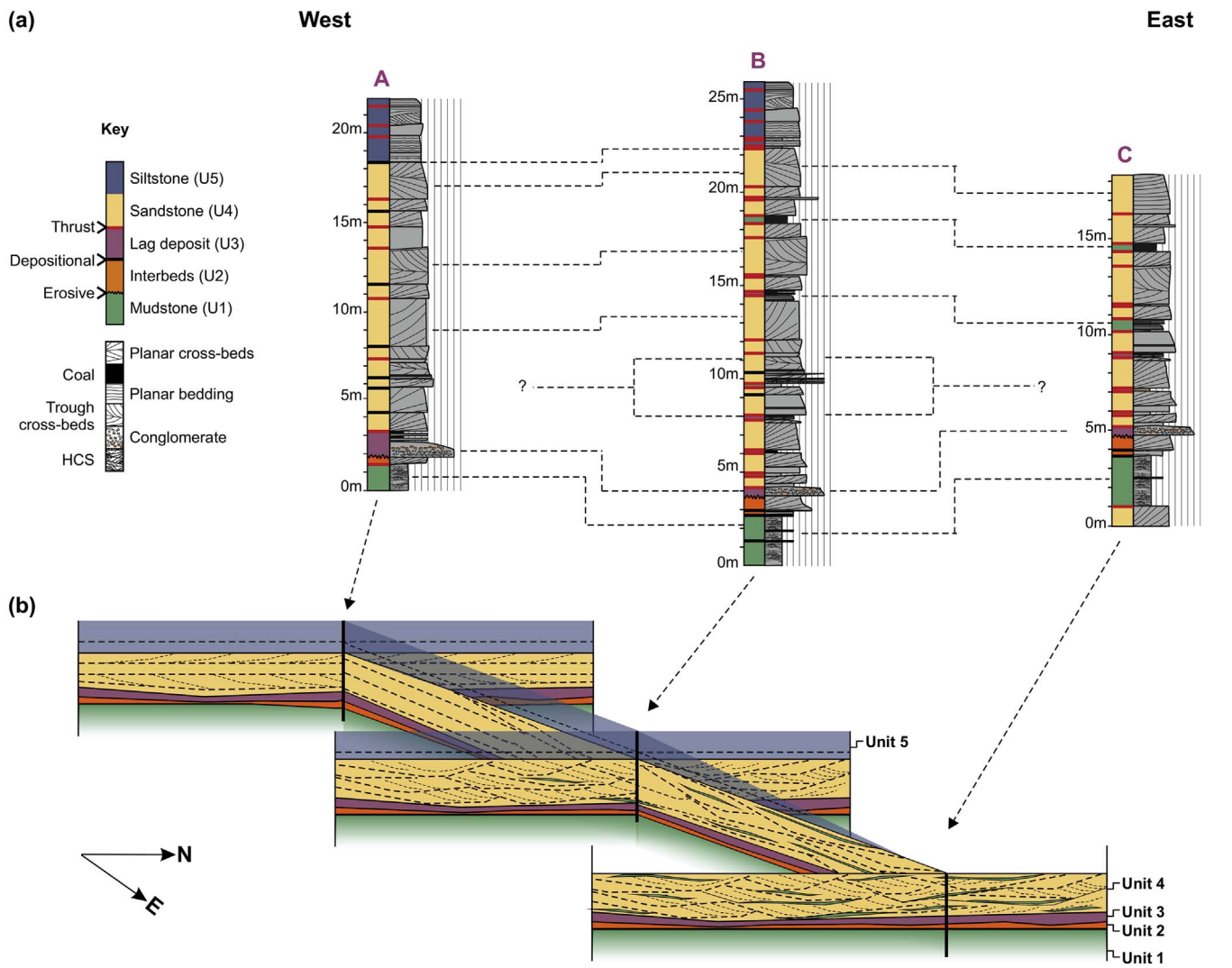


**Fig. 4.** Correlated field logs and interpreted linkage of undeformed sedimentary sequence in 3D. (a) Lateral variation in unit thicknesses and compositions across logged sections (See Fig. 1b for log locations). Unit 4 displays greatest lateral variation, recorded by increased frequency and thickness of mud horizons eastwards. (b) Schematic undeformed succession based on field logs showing variations in sedimentary architecture and the general trend for increased heterogeneity of the sedimentary succession to the E. Multiple slip horizons in field logs and likely lateral thickness changes in units do not allow for restoration of the sections.

likely due to local sub-facies at the time of deposition, and the preservation of different architectural elements such as distributary sub-channels, sheet sandstones, overbank deposits and erosional surfaces.

This unit is characterized by increased heterogeneity of internal composition eastwards. At the western-end of the study area (Log A), Unit 4 is characterized by well-bedded, sheet-like sandstone bodies, with planar bed interfaces and planar-bedded or cross-bedded channels. In the central (Log B) and eastern (Log C) sections of the outcrop, channels are up to 1.5 m thick and commonly bound vertically by erosional lags and mudstone lenses. Channel bodies display either trough or planar cross sets, with width to height ratios of ~10. Channel bodies likely record deposition and local shifting of subsidiary distributary sub-channels and bars within the fluvio-deltaic sequence (Bluck and Kelling, 1963). The gross depositional trend for Unit 4 is interpreted as a transition from sheet (possibly flood) sandstones in the West (log A) to a channel-axial position at log B through to an inter-distributary setting eastwards at log C (Fig. 4).

### 3.5. Upper siltstones (Unit 5)

Unit 5 is a fining-upward siltstone, a continuation of the underlying Monkstone Sandstone, from which the change to siltstone is gradational. Measurements from this unit record a small grain size distribution (3–5 μm) and low variability in Silica content and Gamma Ray measurements (16.8–28.7% and 82–109 cps respectively). Poor exposure of this upper part of the sequence does not allow an estimation of total thickness, but a recorded minimum of 4.6 m. The absence of erosive bed contacts within this unit and the transition to greater homogeneity in the sequence may be suggestive of increasing marine influence at a delta-front position, in contrast to the distributary setting associated with Unit 3 and parts of Unit 4.

## 4. Structural geometry at Monkstone Point

Virtual outcrops were generated of Monkstone Point from 14 Light Detection and Ranging (LiDAR) scans, and by Structure from Motion, using 627 terrestrially acquired digital images. Two virtual outcrops provided high resolution, photorealistic 3D reconstruction (Fig. 1b) of the study site, allowing us to map, in detail, sedimentary and structural features around the outcrop. In addition to virtual outcrops, 154 digital strike and dip measurements (Fieldmove app on iPad 4) and digital imagery of the study site were collected while in the field. Compilation of all datasets into a single geo-referenced 3D framework was performed subsequent to processing, along with logged sections and NGR

data (Fig. 1b). The 3D model was used to create virtual scanlines, and allowed detailed virtual outcrop mapping to be accurately projected onto 3 cross-sections with high precision. Compilation of data in digital space was an important step in the workflow for this study, greatly aiding visualization and structural analysis at a range of scales in 3D, of a morphologically complex study site.

A semi-regional cross-section through part of eastern Pembrokeshire (Fig. 2), compiled from data presented in this study, the work of Jenkins (1962), Coward and Smallwood (1984), and Smallwood (1985), puts the detailed observations, presented here, at Monkstone Point into a broader context. The cross-section highlights variations in structural style from south to north over a ~3 km section. Deformation south of Monkstone, at Trevayne headland, is characterized by a large anticline structure. North of the study area, towards Saundersfoot, deformation is dominated by imbrication of heterogeneous sequences (Fig. 2), interpreted by Smallwood (1985) as due to shallow detachment levels and thin-skinned deformation. Monkstone Point marks the transition between locally homogenous strain accommodation immediately to the south and highly partitioned, thrust-dominated deformation to the north. The main structure at Monkstone Point is an anticline, bound to the S by thrust F1, and northwards by two back-thrusts of opposing vergence (F3) (Fig. 2). In the zone bound by thrusts F1 and F3, the outcrop provides three natural sections across the structure (Figs. 5–7), allowing detailed 3D examination of deformation within the anticline. Three parallel cross-sections (Fig. 8), roughly coincident with the natural cliff lines, were primarily constructed by virtual outcrop interpretation and subsequent polyline projection to N-S oriented cross-sections. Field data, including digital imagery and sedimentary logs, supplemented and improved digital interpretations. The three projected cross-sections, summarizing structural architecture, are described below. Detail of these structures is provided in field photographs (Figs. 5–7) and cross-sections (Fig. 8).

### 4.1. West cliff (cross-section A)

This section is dominated by a S-verging, translated detachment anticline in the upper part of the cliff (Figs. 5 and 8a). This complex structure displays relatively parallel bedding geometries on the outer arc, disharmonic geometries in the core of the fold and an anticline in the footwall to the F2 thrust, in the lower part of the cliff section. Smaller ($\lambda < 2$ m), early detachment folds are present in the outer arc of the structure, and display geometries suggestive of refolding with the development of the major fold (Fig. 9a). Geometries in the core of the structure are defined by a complex pattern of thickened units cut by multiple faults that decapitate smaller, second-order folds. Minor thrust faults are folded throughout the cliff section (Figs. 5 and 9a) and are interpreted as representing early-stage deformation before the development of the larger anticline. In addition, the structure contains a small number of low offset (> 0.2 m), unfolded thrust segments (Fig. 8a) that offset fold limbs and serve to accommodate strain during late-stage contraction.

Translation of the detachment fold along a forelimb thrust (F2), exposes and partially repeats units 4 and 5 in the footwall stratigraphy in the anticline backlimb (Fig. 10a). Similarly, lower offset, subordinate thrust segments within the hanging-wall and footwall of the forelimb thrust F2 repeat parts of the stratigraphy tectonically thickening the sedimentary succession. Unit thicknesses in the Section A log (Fig. 4) thus record both depositional thickness and subsequent tectonic thickening, and are not representative of the true stratigraphic thickness.

### 4.2. Monkstone cave (cross-section B)

The prominent anticline in the hanging-wall to thrust F2 of cross-section A is not preserved at this middle part of the outcrop (Fig. 6). The cross-section exposes a structurally lower part of the sequence: the anticline in the footwall to the F2 thrust is partly exposed at the base of cross-section A (Fig. 8b). Units 1 to 4 outcrop here in this anticline which is truncated to the S by the N-propagating thrust (F1) which marks the southern edge of the thrust-bound anticline (Fig. 2). The S-propagating F2 back-thrust (associated with the translated detachment fold in cross-section A) intersects the northern part of this cross-section

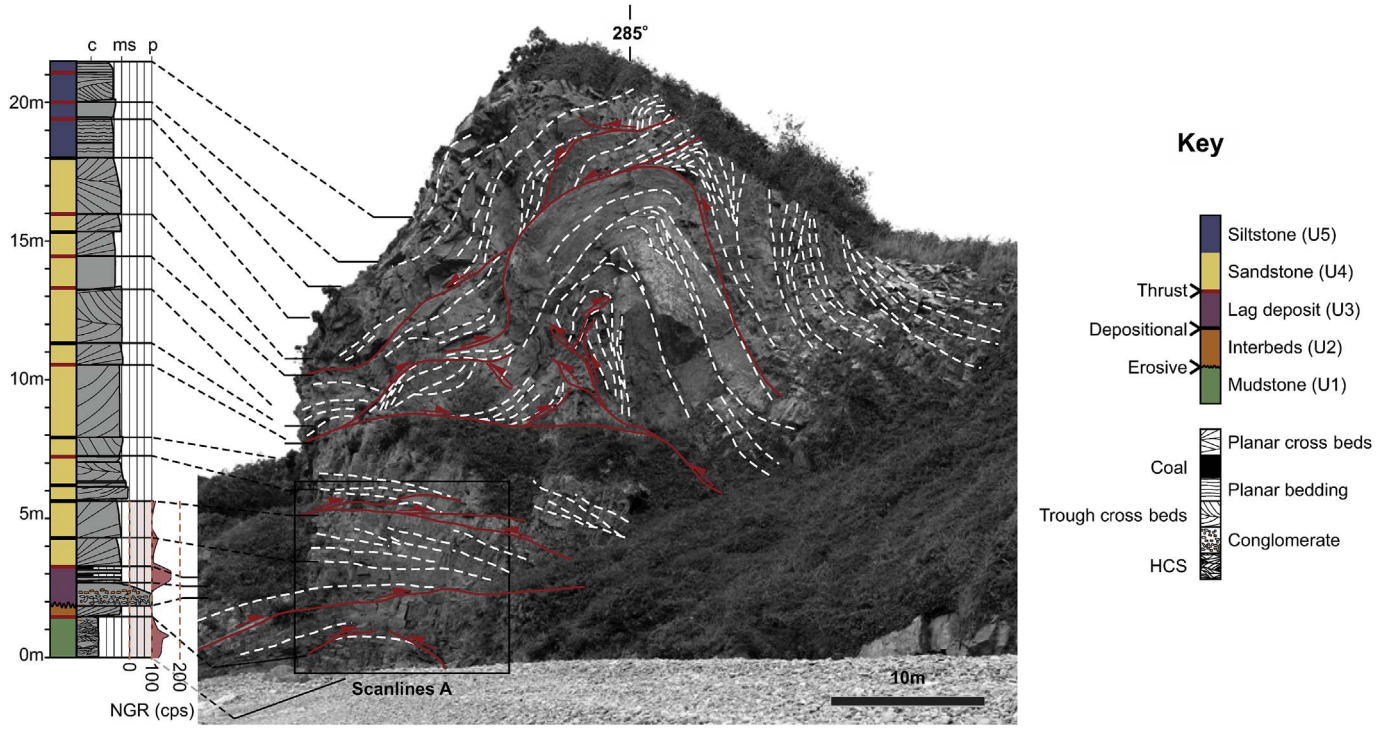


**Fig. 5.** Field photograph and sedimentary/structural log of West cliff section, Monkstone Point (Section Line A, Fig. 1a). Thrusts marked by red lines, bedding in white. NGR data in pink on log. Field photograph corresponds to Section A (Fig. 8a). (For interpretation of the references to colour in this figure legend, the reader is referred to the web version of this article.)

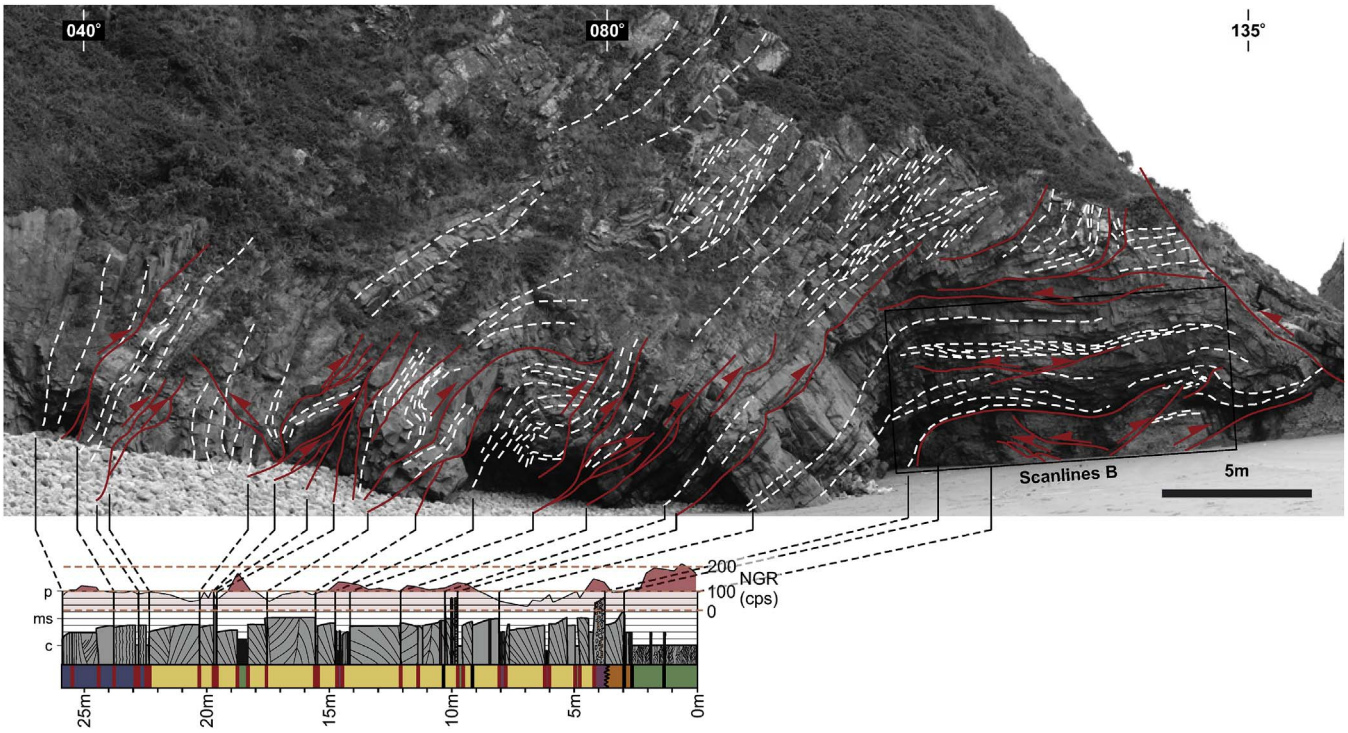


**Fig. 6.** Field photograph and sedimentary/structural log of middle cliff section, Monkstone Point (Section line B, Fig. 1a). Thrusts marked by red lines, bedding in white. NGR data in pink on log. Field photograph corresponds to Section B (Fig. 8b). Key to sedimentary log in Fig. 4. (For interpretation of the references to colour in this figure legend, the reader is referred to the web version of this article.)

and repeats the upper part of Unit 4 (Fig. 8b). Deformation structures vary according to stratigraphic position (see Section 5) and mechanical units record relatively uncoupled deformation (Fig. 9c) compared to cross-section A. The basal detachment (in Units 1 and 2) is exposed in the base of the cliff, while higher in the sequence Units 3 and 4 are deformed by low amplitude folding and thickening (Fig. 10b).

Channels are commonly trough cross-bedded and display low width to height ratios (~10), with erosional bases commonly lined by mudstone lenses and gravel lag deposits (Fig. 9b). Bedding plane interfaces are discontinuous and contain asperities related to erosive boundaries. Strain is largely accommodated by bedding-plane slip surfaces, which are linked by bed-internal thrust ramps. The majority of channels here are trough cross-bedded, and provide weak planes along which these thrust-ramps branch into and propagate along (see Section 5.4), linking detachment horizons above and below (Fig. 9b). Units 3, 4 and 5 are also deformed by large wavelength folding above the detachment in Units 1 and 2 below (Fig. 10b). Higher in the section, Unit 5 is poorly exposed, but does not record the minor, second order detachment folding observed in this Unit at cross-section A (Fig. 10b).

### 4.3. East cliff (cross-section C)

This part of the outcrop provides the longest of the three natural N-S cross-sections (Fig. 7), at the eastern end of the Monkstone anticline

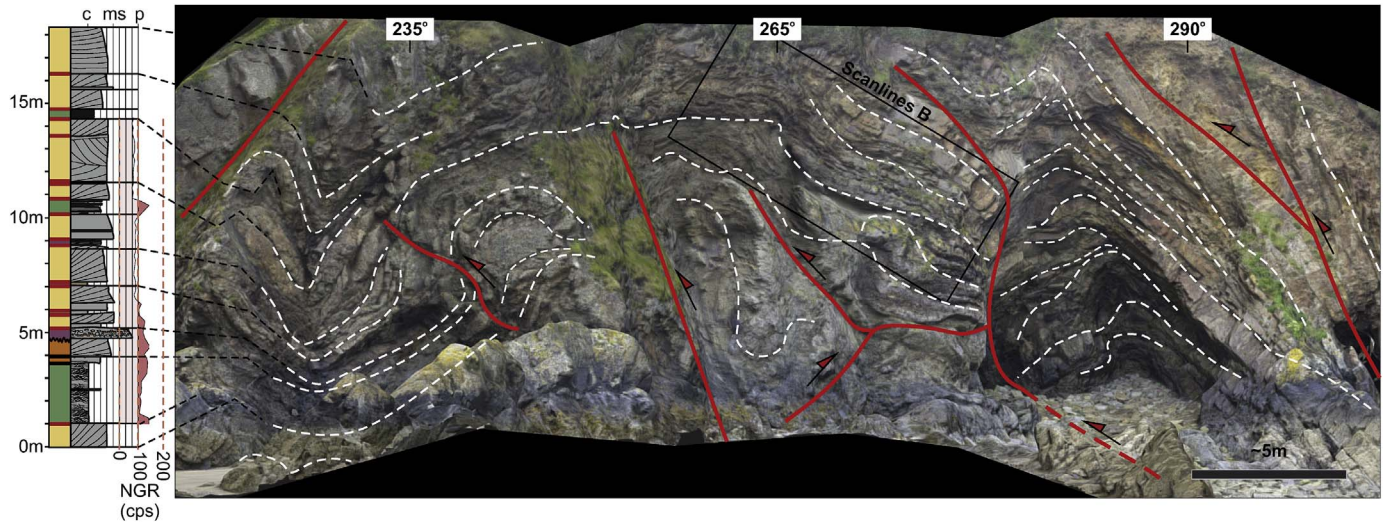


**Fig. 7.** Virtual outcrop image and sedimentary/structural log of East cliff section, Monkstone Point (section line C, Fig. 1a). Thrusts marked by red lines, bedding in white. NGR data in pink on log. Image corresponds to Section C (Fig. 8c). Key to sedimentary log in Fig. 4. (For interpretation of the references to colour in this figure legend, the reader is referred to the web version of this article.)

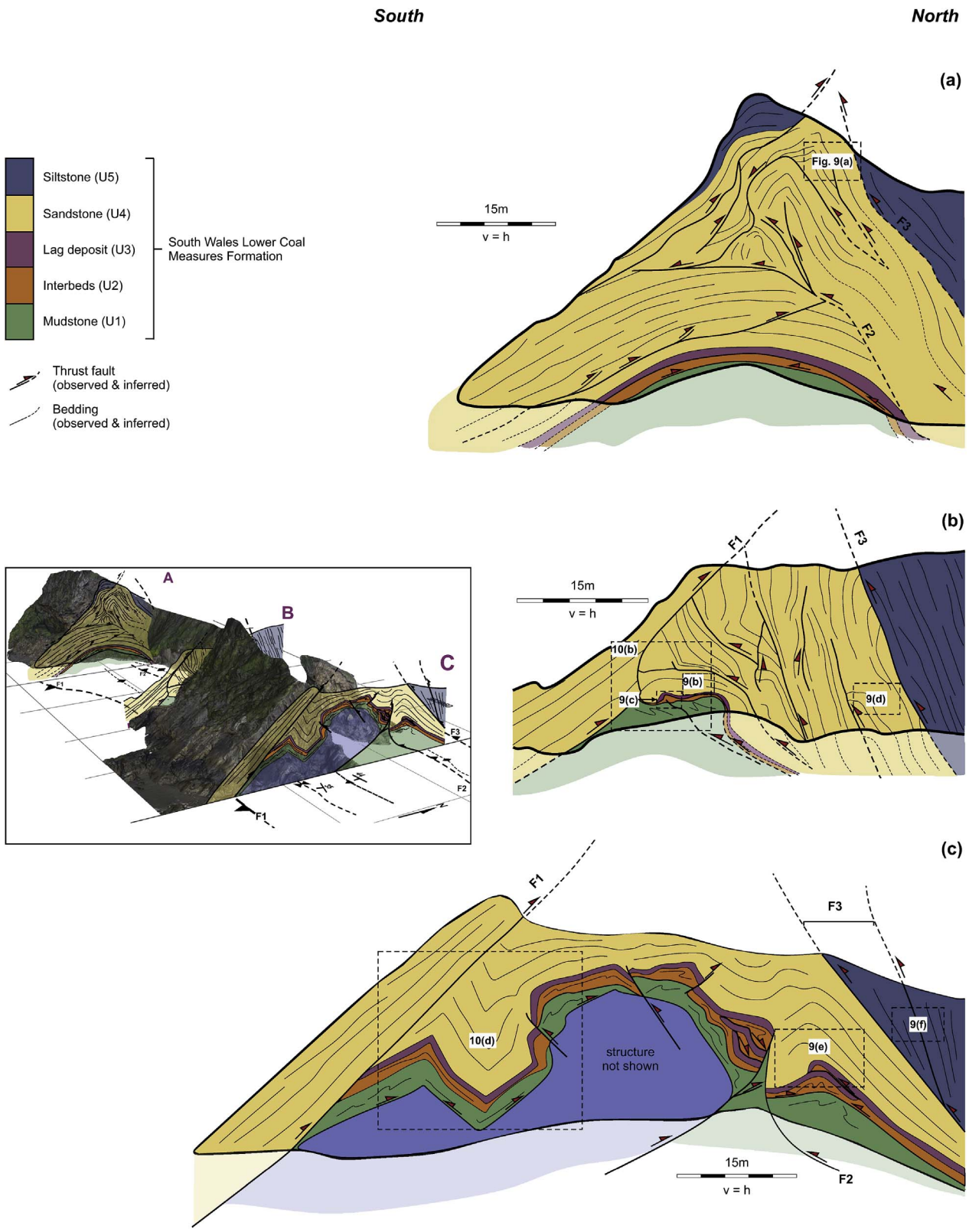


**Fig. 8.** Sequential cross-sections from Monkstone Point. Inset shows approximate locations of cross-sections, with reference to virtual outcrop reconstruction of study area. Dashed boxes and numbers on cross-sections reference figure numbers for field photographs at corresponding locations on the outcrop. F1, F2 and F3 are named thrusts in the study (see Fig. 2 for regional cross-section).

outcrop. Structural style is broadly similar here within the individual units, though there is a trend for greater complexity and variety of structural features throughout (Fig. 8c). Deformation within the northern and southern limbs of the larger Monkstone anticline is mainly accommodated by detachment folds (Fig. 8c) and thrusts. The southern limb of the anticline is formed by the laterally continuous N-propagating thrust (F1) present in all sections; similarly, the structure is bound to the N by thrust F3. The folds at cross-section C are internally

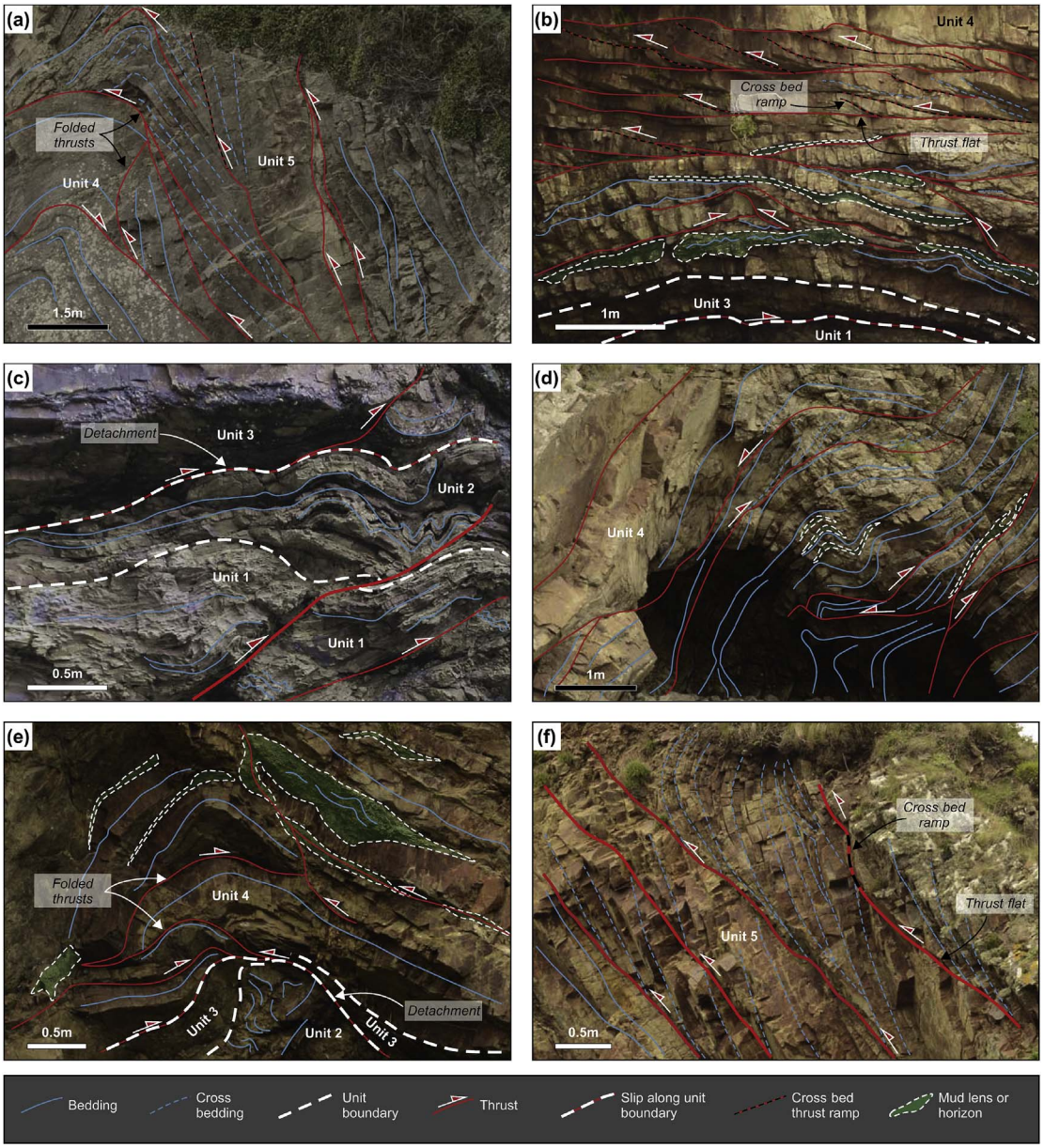


**Fig. 9.** Field photographs, with interpretations, of meso-scale deformation structures at Monkstone Point. Photograph locations referenced in Fig. 8. (a) Refolded early thrusts in upper part of cliff, cross-section A. (b) Channel bodies in Unit 4 display cross-bed thrust ramps and bed-interface thrust flats here, at cross-section B. (c) Units 1 and 2 thickened and disharmonically folded in the anticline core, below a detachment horizon. Unit 3 above apparently relatively undeformed above. (d) Disharmonic folding in Unit 4 where thin muddy horizons are present. Thrust propagation and fold vergence to N and S. (e) Increased frequency of muddy lenses and layers (in green) through the sedimentary sequence eastwards recorded at cross-section C. Thrusting and tectonic stacking of Units 3 and 4, later folded by the larger fold structure (see cross-section C, Fig. 8c). (f) Cross-bed thrust-ramp geometries in the lower part of Unit 5. Thrust segments record low offset (> 0.05 m). (For interpretation of the references to colour in this figure legend, the reader is referred to the web version of this article.)

complex, asymmetrical and display vergence to N and S. This lack of symmetry is attributed to three factors: (1) laterally discontinuous geometries of individual sedimentary bodies, imparted by original deposition results in fold limbs of non-equal thickness (Figs. 9e and 10d). Strain in the core of folds is accommodated by thickening and folding of fine-grained material. Where fine interbeds are present in fold cores, disharmonic folding is present (Fig. 9e). (2) Tectonic stacking of units and small scale detachment folding during early deformation similarly results in non-planar bodies being incorporated into folds and thus differential fold limb thicknesses (Fig. 10d). (3) Late-stage fold modification by thrusting further adds to structural complexity by translating and rotating fold limbs (Fig. 10c).

## 5. Mechanical stratigraphy

An abundance of meso-scale structures at Monkstone Point allows detailed assessment of the layer-by-layer structural style, its evolution and consequently characterisation of the mechanical stratigraphy. This section aims to evaluate the observed patterns of deformation internal to each unit, at unit interfaces, and through the exposed sequence. To assess lateral variations in sedimentary architecture and impacts on the assigned mechanical stratigraphy, virtual scanlines (Fig. 11, and locations of scanlines, Figs. 5–7) were used to record the frequency and spacing of thrust faults or fault segments (discrete slip surfaces) through units in each of the cross-sections. This was carried out by digital mapping of fault segments on the virtual outcrop along parallel scanlines through Units 1–4. Measured fault offsets and approximate

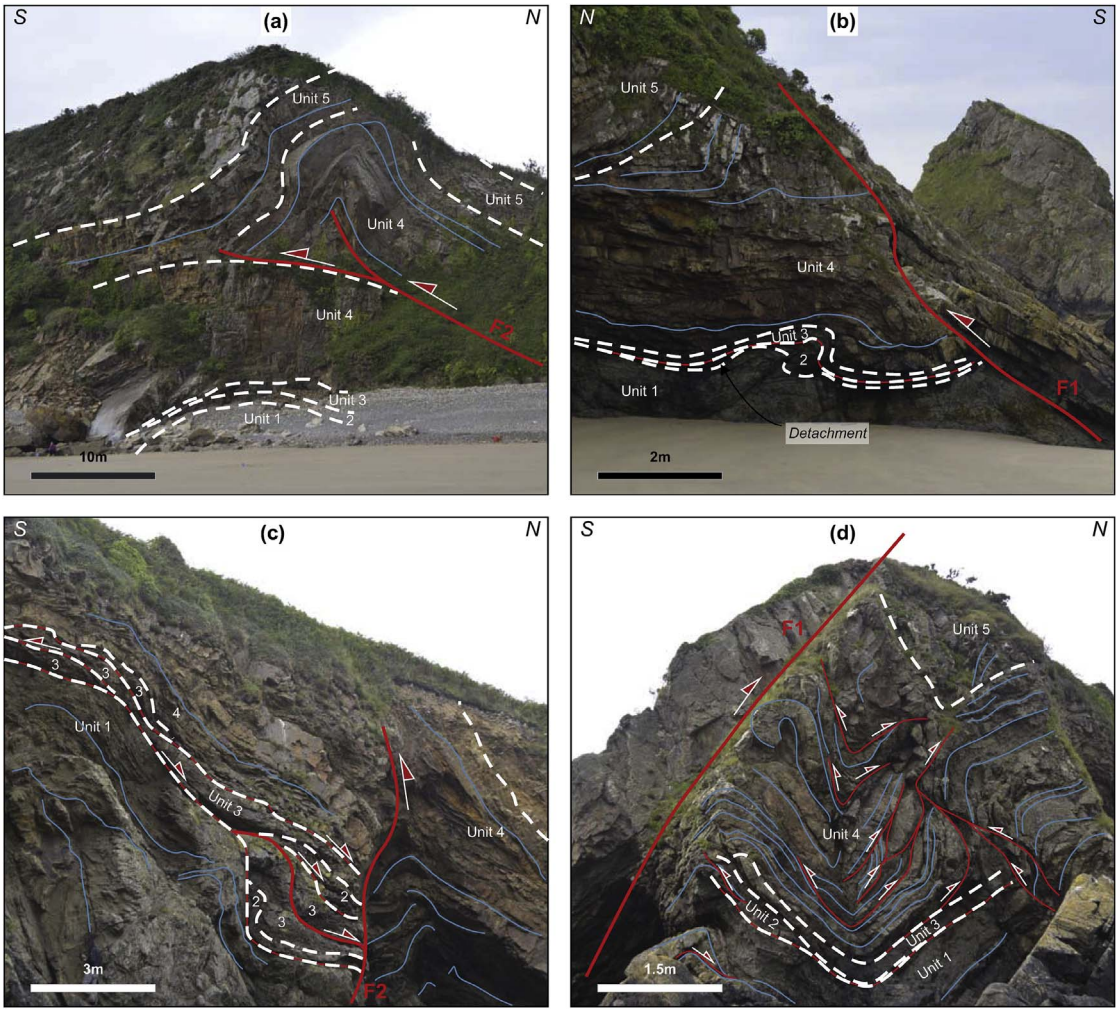


**Fig. 10.** Structural arrangement of units at Monkstone Point. (a) Oblique view of cross-section A (Fig. 8a), showing some repetition of Unit 4 in the hanging wall of thrust F2. (b) Field photograph of cross-section B. Vertical changes in structural style recorded in mechanical units (See Section 5). Main detachment above Unit 1 & 2 in centre of image. (c) Field photograph of part of cross-section C (Fig. 8b). Tectonic stacking of Units 2 and 3, abutting the southern limb of detachment anticline at cross-section C. (d) Syncline at southern edge of cross-section C (see Fig. 8 for location). Field relationships record thrusting and tectonic stacking that pre-dates folding of the sequence. White numbers on images refer to unit numbers in text.

positions of fault-scanline intersections is presented in Fig. 11. We combine the scanline data with sedimentary logs, cross-sections and field observations to assess the link between sedimentary architecture and observed partitioning of strain.

### 5.1. Unit 1

Unit 1, the marine mudstone unit at the base of the studied stratigraphic sequence, is deformed in the core of the anticline in the footwall to thrust F2 by internal folding and small-scale thrusting (Fig. 9b). The interpreted detachment horizon at the top of Unit 1 (Fig. 10b) coupled with small-scale disharmonic folding and low-offset thrusting (Fig. 9c) within the Unit may suggest tectonically induced thickness changes. Lack of exposure at the base of this unit, however, does not allow for any estimation of original thicknesses. Respective minimum and maximum recorded thicknesses of this unit of 0.4 m on the outer arc of the syncline in cross-section C (Fig. 9d), and > 2.1 m in the core of the anticline in the footwall to thrust F2 (Fig. 9c) thus do not provide any diagnostic information regarding deformation-related thickness changes.

Unit 1 shows little lateral variation in internal structural style. Intersected fault segment frequencies (2.1/m, 1.5/m, 2.3/m respectively) and average displacements (9.1 cm, 9.3 cm and 6.4 cm respectively) across scanlines A, B and C are relatively consistent in the three scanlines (Fig. 11), recording little systematic variation laterally. This style of deformation is consistent throughout the outcrop and no evidence was found to suggest significant lateral variations in the mechanisms for strain accommodation within Unit 1.

### 5.2. Unit 2

Unit 2, a discontinuous package of alternating thin sandstone and mudstone units (up to 0.6 m thick) lying directly above the marine mudstone of Unit 1, contains a variety of deformation structures. Strain is typically accommodated in the more competent sandstone intervals by minor disharmonic folds ($\lambda$ = 0.01m-0.13 m), which verge to the N, and are commonly disjointed and rotated by small scale thrust imbrication (Fig. 9c), with a recorded average intersected thrust frequency of 0.8/m (Fig. 11). Detachments to small-scale thrusts within this package are concentrated along mudstone intervals (Fig. 10d), with thrust ramps that climb up through thin sandstone interbeds. Small-scale structural features within Unit 2 are generally self-contained within this interval; thrust traces and axial planes of folds are commonly bed-bound (Fig. 9e). Where this unit is deformed by through-going thrusts (Fig. 9c), scanline data (Fig. 11) record an increase in fault offset and frequency within Unit 2. Field observations (Figs. 9 and 10) and sedimentary logs (Fig. 4a) capture the laterally discontinuous nature of Unit 2; thickness changes alone are thus not diagnostic of

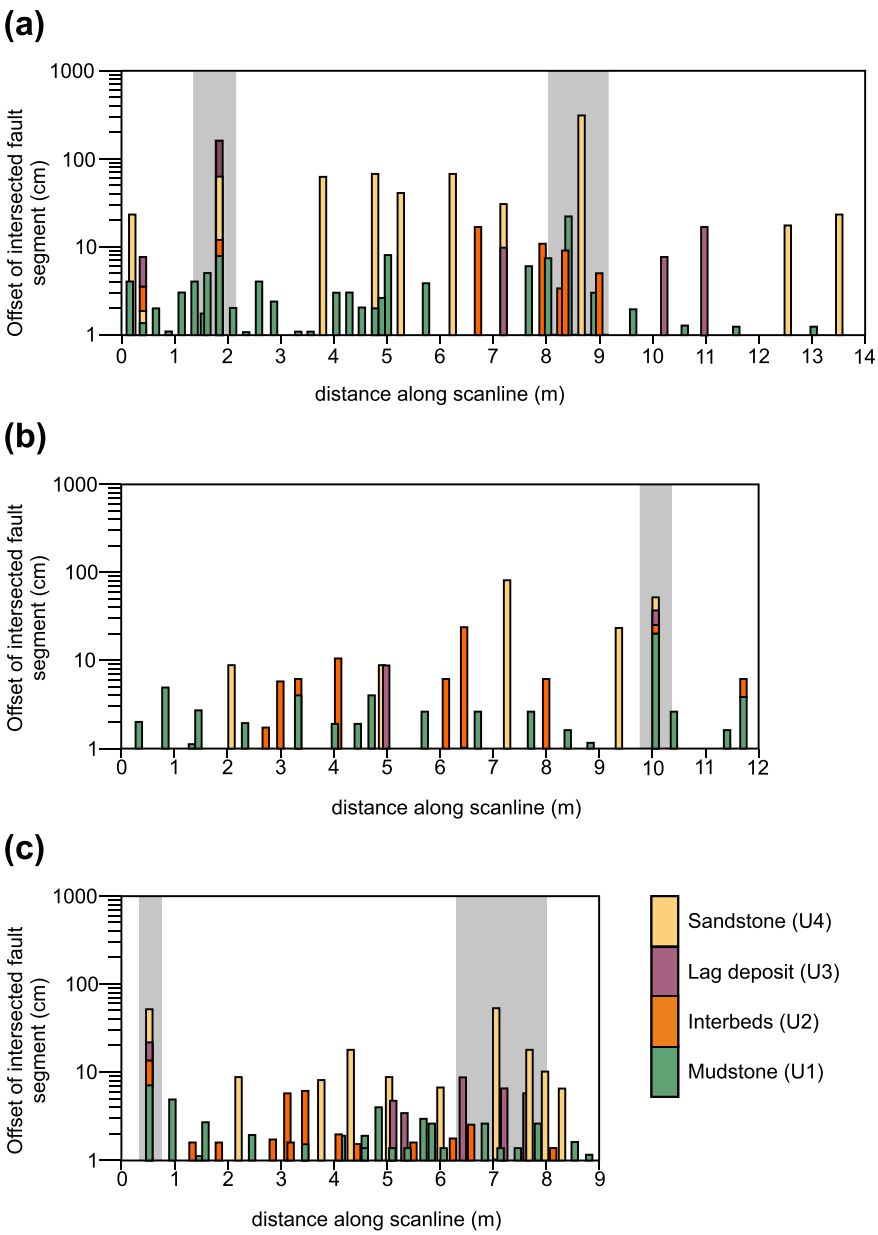


**Fig. 11.** Measured displacements of all mapped faults across virtual scanlines. For scanline locations, see Figs. 5–7. Each colour bar represents a measured fault, with offset, within mechanical units. Zones with clusters of faults (shaded grey) and stacked bars record larger thrusts that deform the entire sequence. (For interpretation of the references to colour in this figure legend, the reader is referred to the web version of this article.)

deformation. Unit 2 is thickened in the exposed core of the larger anticline, evident from internal folding of the unit (Fig. 9c and e), and possibly thinned on the outer arc of the exposed syncline (Fig. 10d). Thrust flats are concentrated within Unit 2 (where this unit is present). Where Unit 2 is absent from the sedimentary sequence (e.g. Fig. 9b) due to non-deposition or downward incision of Unit 3 (e.g. Units 1 and 3 are in direct contact) evidence of layer parallel slip is common, with thrust flats concentrated along the interface of Units 1 and 3 (Fig. 4a, log A). As with Unit 1, structural style in Unit 2 is relatively laterally consistent. Scanline data for Unit 2 do not show systematic lateral variation in unit-internal thrust fault distributions (Fig. 11). Thrust segments do, however, display higher frequency and lower displacements at scanline C, though this likely reflects the greater thickness of Unit 2 at this eastward position.

### 5.3. Unit 3

Unit 3, the sheet gravel lag unit is deformed, as with the lower two units, by several fold and thrust structures. Where larger-scale thrusts propagate through the sequence, or folding of several units occurs, brittle structures dominate the style of deformation, rather than the semi-ductile thickness changes and unit-internal folding observed in the sequence below (Units 1 and 2). In the syncline and anticline cut by cross-section C, the unit is deformed by folding (Fig. 10d). Unit 3 records relatively little deformation by thickness change, but is deformed by folding (Fig. 10b) or tectonic stacking and thrust imbrication (Fig. 10c).

Unit 3 incises downwards into Units 1 and 2 and displays greater lateral variations in structural style than these lower units. Scanline A and B show that Unit 3 is generally unaffected by smaller-scale deformation structures dominant in the finer-grained units below but appears to be mechanically coupled, in places, to Unit 4 above. Where the transition to Unit 4 is gradational, thrust segments do not branch into lower angle, bedding parallel thrust flats at the unit boundary, but maintain high angle ramp orientations. At these gradational contacts, Units 3 and 4 appear to be deformed by low amplitude folding, with multiple detachments in the fine-grained Units 1 and 2 below (Fig. 10b). Abrupt changes in composition or grain size between this unit and the overlying sequence (Fig. 10d), or the presence of thin mud-drapes at the boundary between these units, results in a decoupling

effect, where deformation is accommodated by thrusts and duplex formation within Unit 3 (Fig. 10c).

### 5.4. Unit 4

This sandstone-dominated part of the stratigraphic sequence has the greatest lateral variability in sedimentary architecture, unit-internal composition and style of deformation. At cross-section A, this unit is well bedded and mapped bed interfaces display greater lateral continuity than at the other cross-sections (see Figs. 5 and 10a). Cross-section A (Fig. 8a) and log A (Fig. 4) show low angle cross-sets or parallel bedding and relatively little variation in grainsize (see Section 4) through Unit 4 at this position (Fig. 4a, Log A). Apparently distributed deformation in this part of the succession at cross-section A (Fig. 8a) may relate to the observed trends here for little variation in grainsize and composition: while there is not an absence of small-scale structural features, large scale folding and thrusting dominate deformation. The relatively simple, distributed deformation observed in cross-section A is contrasted in cross-section B by patterns of increasingly partitioned strain in Unit 4. Strain is accommodated along pre-existing zones of weakness; the majority of channels here are trough cross-bedded (Fig. 6), and provide weak planes along which thrust-ramps branch, propagating from bedding plane detachments (Fig. 9b).

Internal deformation in Unit 4 at cross-section B is dominated by internal thickening and tectonic stacking of channel bodies, rather than by folding, as recorded at cross-section A. Thrust flats are concentrated along channel bases, with branch points into ramps located at bedding-plane and cross-bed intersections (Fig. 9b). Individual ramp segments in thrusts of this type have very low offsets ($> 0.02$ m), and generally terminate within channel bodies, rather than propagating upwards into the next channel body. Where these ramps are hard-linked to overlying slip surfaces, imbrication occurs, and individual slices take on sigmoidal geometries within these meso-scale duplexes. At cross-section C, Unit 4 is primarily deformed by tighter folding (Figs. 9e and 10d) than observed in the other sections. This style of deformation is suggestive of high ductility contrasts (Ramsay, 1974) within Unit 4. Greater abundances of intra-formational muds, recorded in log C (Fig. 4a) may provide planes of low frictional strength between sandstone beds and allow tighter folding (Ramsay, 1974). In contrast, at cross-sections A and B, where Unit 4 is characterized by higher sandstone to mudstone ratios (see Figs. 5–7 for logs), folding appears to occur at a longer wavelength within this unit.

The variability of strain accommodation structures recorded in Unit 4 suggest that subtle changes in the composition of this unit, both laterally and vertically, determined how the unit deformed during contraction. Recorded structures suggest that the composition of this part of this succession (beds and bed interfaces) and the organization of these components impacted the partitioning of strain. Structural style in this unit is thus highly sensitive to its compositional variation in 3D (Fig. 12).

### 5.5. Unit 5

The uppermost unit of the sequence exposed at Monkstone point, Unit 5, records deformation by tectonic stacking, bedding plane detachments and small-scale detachment folding (Fig. 9a, f). Stratigraphic thickness of this poorly exposed unit is not known here, as the upper limit of the unit is not exposed at Monkstone Point.

## 6. Evolution of deformation and mechanical stratigraphy

In addition to lateral variations in the mechanical stratigraphy at Monkstone Point, the distribution and cross-cutting relationships of structural features allows the structural evolution during Variscan deformation to be determined. The evolution of deformation, structural style and mechanical changes are described below.

1. Bedding slip surfaces, deformed by later fold structures in Units 2–5 (Figs. 9 and 10) provide evidence that early deformation was dominated by layer-parallel shortening (Fig. 13). This suggests that strain was highly partitioned at the onset of contraction, with little mechanical coupling between units. Deformation is concentrated along layer-parallel zones of pre-existing weakness, such as bed contacts lined with coal or fine-grained material (Fig. 4a).
2. Early to mid-stage deformation is recorded by unit-bound meso-scale structures. Distinct structural styles are recorded in each mechanical unit (Section 5) e.g. thickening and disharmonic folding in Units 1 and 2, thrusting and tectonic stacking in Units 3 and 4, and small-scale detachment folding in Unit 5. Variable mechanical coupling of units is dependent on local facies architecture, which influence local patterns of strain distribution. Where bed and unit boundaries record abrupt compositional changes, strain is localised onto discrete fault planes, whereas gradational changes result in distributed deformation and meso-scale structures that record deformation across units.
3. Larger-scale detachment folding deforms earlier fold and thrust structures (Fig. 10b) in Units 3, 4 and 5. Units 1 and 2 are thickened in anticline cores (Fig. 9e) and thinned on syncline outer arcs (Fig. 9d), suggesting that these stratigraphically lower, fine-grained units represented a weak detachment layer for folding of overlying Units 3, 4 and 5. This stage marks a transition from highly partitioned, unit-internal deformation to more homogenously distributed strain and the mechanical coupling of Units 1 and 2, and Units 3, 4 and 5 respectively (Fig. 13).
4. Large-scale thrusts that cut through the entire sequence, including meso-scale structures (Fig. 10b, d), suggest that there was a clear transition from early, unit-internal deformation and layer-parallel-slip to the formation of larger structures that deformed the entire sequence. Translation of detachment folds along a thrust forelimb deform the entire sequence (Fig. 8). Through-going late-stage thrust faults are associated with clustered fault segments on scanlines and are zones of relatively high fault displacement (Fig. 11). This clustering of fault segments occurs in all mechanical units (Fig. 11), but unlike the major through-going thrusts that cut and deform the exposed stratigraphic sequence, the clustered, smaller displacement, faults are unit-bound. The through-going faults complete the transition from uncoupled, unit-partitioned strain during early deformation to distributed deformation and outcrop-scale folding during mid-stage deformation, and finally to highly localised strain along through-going faults, which deform the entire sequence during late stage deformation (Fig. 13).

## 7. Discussion

Hancock et al. (1982) recognised the superimposition of folds and thrusts on original sedimentary structures at Monkstone Point, and elsewhere in SW Wales. Employing a multi-scale 3D approach we have attempted to detail, using Monkstone Point as an example, how such sedimentary-structure interplay works. The findings allow refinement of regional, 2D end-member models of distributed vs partitioned strain in the sedimentary succession of SW Wales.

### 7.1. Linking sedimentary facies and structural style

Our results show that the lower, finer-grained part of the sequence (Units 1 and 2) provided a weak detachment layer for the coarser-grained units above. These two units probably represent lagoonal or marginal marine deposits, their fine-grained nature creating the weak detachment. This observation is in agreement with observations made of Variscan deformation exposed in other areas of the UK (e.g. Lloyd and Chinnery, 2002) and more generally, with fold and fault detachments observed to concentrate in fine-grained material (e.g. Woodward and Rutherford, 1989). There is relatively little lateral variation in the

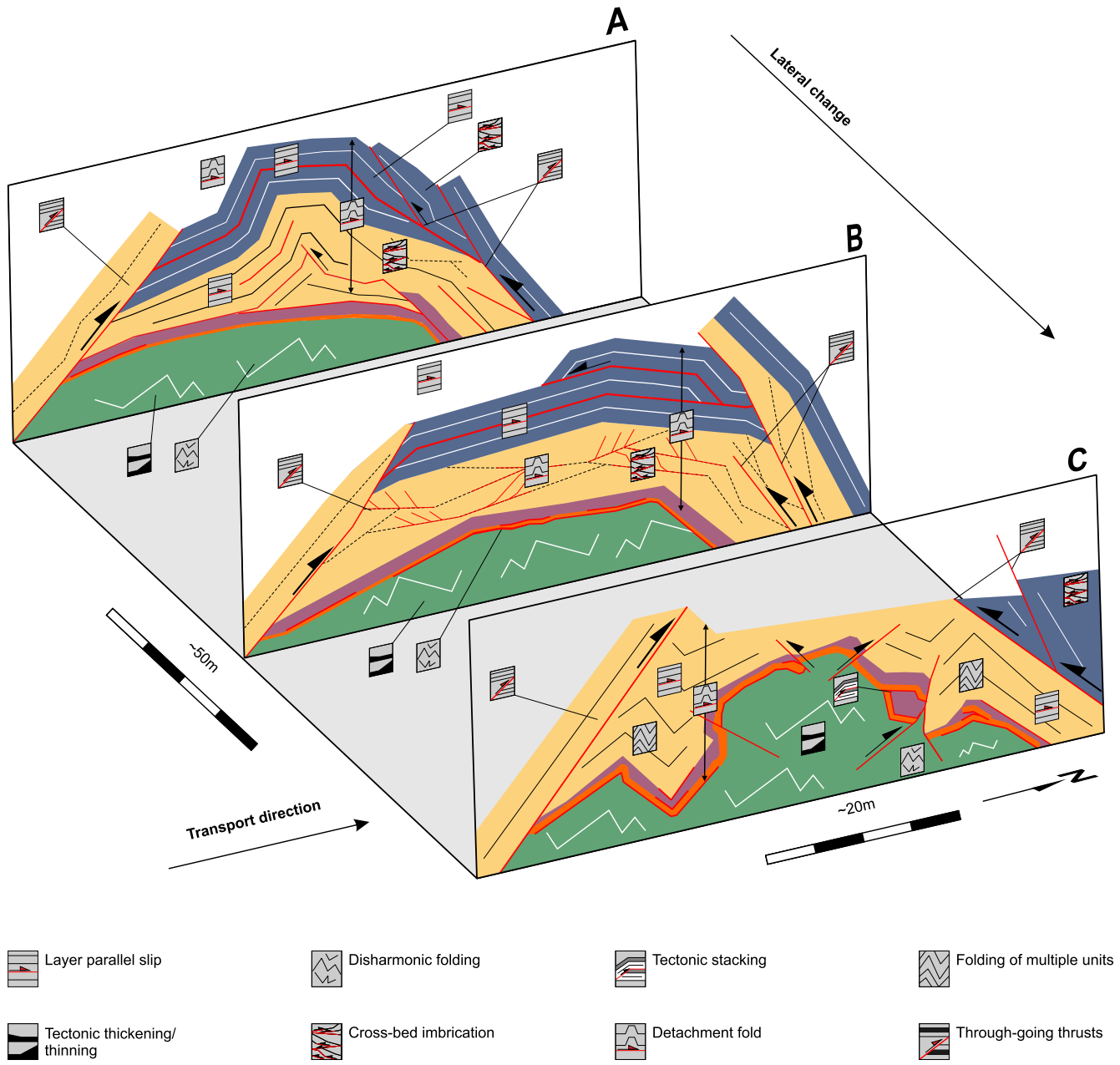


**Fig. 12.** 3D distribution of meso-scale deformation structures across the 3 cross-sections at Monkstone Point. Grey cartoon boxes on schematic records dominant deformation mechanism at that location.

mechanical behaviour of Units 1 and 2. Similarly, Unit 3 records little lateral variation in structural style (Section 5.3), and predominantly deforms by low amplitude folding or internal thrust-stacking that tectonically thickens this unit. The sandstones and siltstones of Units 4 and 5 show greater 3D variation, in both sedimentary architecture (Section 3) and patterns of strain distribution (Section 4). At the western edge of the outcrop (Fig. 4, log A), gradual vertical transitions in grain-size and grain composition, coupled with planar bed boundaries are possibly suggestive of a depositional environment with some marine influence (George, 2000), which has the effect of homogenising the succession. This sedimentary homogeneity results in distributed deformation within the unit, particularly after early-stage, layer parallel slip deformation (see Section 6). Deformation in these units is dominated by a large fold structure (Fig. 5) that deforms the upper part of the stratigraphic succession (Units 3, 4 and 5). Small-scale deformation structures such as cross-bed thrusts (Fig. 9b) or minor detachment folds (Fig. 9a) are not absent here, but are subordinate to the larger fold-thrust structure.

At cross-section B, greater stratigraphic heterogeneity results in changes in structural style. Mud lenses, gravel lags and erosional surfaces (Fig. 4a, log B) within Unit 4 are suggestive of a greater fluvial influence here than at cross-section A, and either a position more axial to a distributary channel, or a more proximal setting. The abrupt change in sedimentary architecture from cross-section B, ~100 m away, is likely explained by small-scale lateral variability in a distributary fluvio-deltaic system, common in the Carboniferous in SW Wales (George, 2000). The eastern part of the outcrop, at cross-section C, is characterized by a greater abundance of and increased thicknesses (up to 30 cm) of muddy horizons within Unit 4, a factor that defines structural style. The muddier parts of the sequence likely represent an inter-distributary setting. This change in deposition and the associated increased stratigraphic heterogeneity of the sequence is reflected in increased complexity of the structural style and the occurrence of tight folds (Fig. 7) at cross-section C.

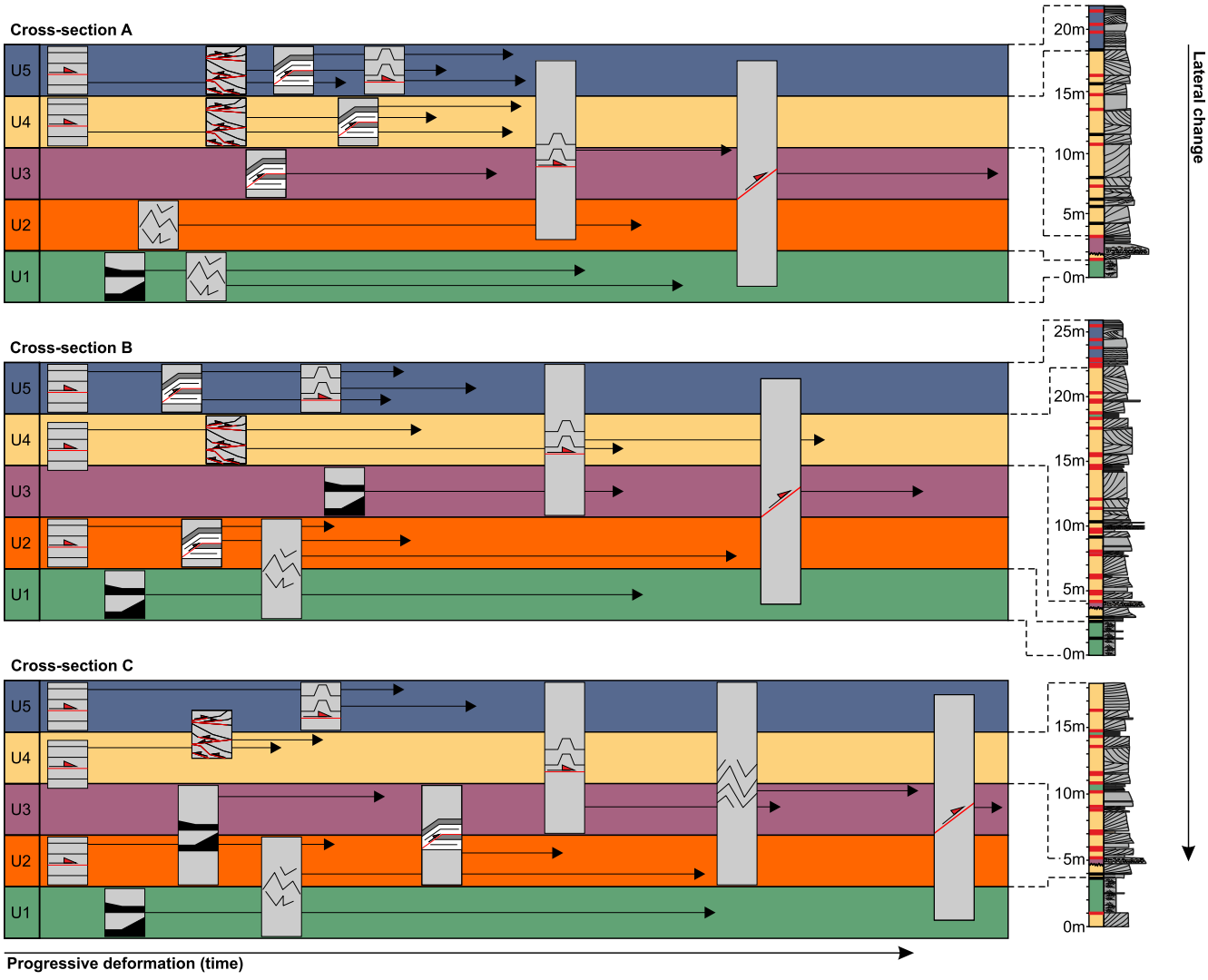


**Fig. 13.** Temporal evolution of the mechanical stratigraphy, recording the transition in structural style and patterns of strain distribution through structural evolution. Grey boxes denote dominant deformation mechanism in mechanical units during progressive deformation (for symbols, see Fig. 12). Temporal extent of deformation marked by horizontal arrows. Where multiple mechanical units are deformed by the same process, grey icons cover a larger vertical area.

### *7.2. Implications for structural and stratigraphic linkage in other settings*

This paper uses the sedimentary architecture in the Upper Carboniferous fluvio-deltaic sequence at Monkstone Point and its subsequent deformation to explore the link between sedimentary architecture and deformation partitioning in multi-layers. Our observations and interpretations are relevant to other multi-layer sequences. The interplay between sedimentary architecture and structural development has been recognised by others: changes in composition through a sequence may influence structural style vertically (e.g. Vergés et al., 2011). Variation in sedimentary thicknesses and unit compositions may control structural style and the localisation of thrusting (e.g. Woodward and Rutherford, 1989). The temporal evolution in mechanical stratigraphy (Fig. 13), and the transition from unit-partitioned to distributed deformation through time has been recognised by others (e.g Hayes and Hanks, 2008; Laubach et al., 2009). Critically, the majority of such studies address this link in 2D, without fully considering 3D variations in strain partitioning at all scales. The multi-scale, 3D approach used in this study has allowed characterisation of deformation patterns vertically through the sedimentary succession, and importantly, has allowed us to record lateral structural variations in mechanical units, as influenced by sedimentary architecture (Fig. 12).

Impersistence of smaller-scale contractional features combined with lateral and vertical variation in the sedimentary architecture that controls this deformation, however, presents difficulties in building a full picture of the 3D deformation at all scales. The level of detail afforded by virtual outcrops (e.g. Bistacchi et al., 2015; Cawood et al., 2017), and the ability to digitally map sedimentary facies (e.g. Rarity et al., 2014), and meso-scale structures (e.g. Martín et al., 2013) mean that these are important tools for 3D analysis. Compilation of the datasets using multi-scale, high-resolution data allowed initial links to be made between sedimentary facies and structural style at Monkstone Point. The use of this technology constitutes an important step in the ability to examine detailed stratigraphic/structural linkage in 3D, as we have done by digitally mapping, in detail, the study area. Although the intricacies of spatial and temporal variations in 3D mechanical stratigraphies will differ according to geological factors unique to each site, the interplay between deposition and deformation recorded in this study is likely to be applicable to a number of geological sites and settings.

Our results provide an insight into the mechanisms of strain localisation at the outcrop scale and support the findings of previous outcrop studies at a range of scales (e.g. Butler, 1992; Roche et al., 2012) showing that vertical and lateral variations in the mechanical properties of stratigraphy will influence fault and fold development and linkage. Work on early high resolution seismic data (Mansfield and

Cartwright, 1996) shows thrust fault initiation in specific layers that link to create through-going thrust faults; indicative, as Pfiffner showed in outcrop (Pfiffner, 1985), of thrust fault tips propagating downwards as well as upwards. More recent work on higher resolution seismic data of deep-water fold thrust belts (e.g. Higgins et al., 2009; Totake et al., 2017) show that fold-thrust systems have complex 3D evolution patterns with strain localised at different levels and in different layers along strike. The advent of such high resolution seismic data and its detailed interpretation begins to provide opportunities for using the 3D complexities observed in outcrop and captured here in a virtual outcrop model, to inform subsurface structural interpretations. Existing 2D models of deformation and assumptions of laterally homogenous stratigraphy require refinement. This refinement requires consideration of internal complexity within mechanical units and the 3D nature of the mechanical stratigraphy as a whole.

## 8. Conclusions

1. Multi-scale outcrop data of a deformed multi-layer at Monkstone Point, SW Wales highlights complex patterns of strain partitioning, and shows that there are a number of factors that may control spatial and temporal variations in how strain is distributed.
2. Variations in internal architecture and composition of the sedimentary sequence, controlled by depositional environment, impacts on where strain is localised. In each of the serial cross-sections, each mechanical unit records a distinct structural style, defined by the composition and internal structure of that unit, and the nature of the interfaces between units. Structural style thus changes vertically through each of the cross-sections.
3. In addition to changes in structural style through the vertical succession, each of the closely spaced (< 100 m), serial cross-sections records significant differences in structural style in laterally equivalent successions. Lateral changes within units, in composition (e.g. relative abundances of fine-grained material), internal structure (e.g. the occurrence of cross-bedding) and architecture (e.g. lateral extent of fine-grained horizons) impacts on where deformation is localised.
4. Temporal evolution of the mechanical stratigraphy records a transition from early, unit-partitioned meso-scale deformation to mid-stage distributed strain to late-stage, highly localised strain along discrete fault planes, which deform the entire sequence.
5. This study shows how mechanical stratigraphy varies not only vertically through a succession, but both laterally and through progressive deformation. Additional studies such as this may refine existing 2D structural models which assume internally homogenous layer cake stratigraphy.

## Acknowledgements

This study was carried out as part of a University of Aberdeen provided PhD supported by The NERC Centre for Doctoral Training in Oil & Gas, (grant reference: NE/M00578X/1). Thanks to Yukitsugu Totake for field assistance and acquisition of images for photogrammetric virtual outcrop generation. Midland Valley Exploration is thanked for academic use of Move 2016 software. We gratefully acknowledge the detailed and constructive reviews by Adrian Pfiffner and Cara Burberry which greatly improved the manuscript.

## Appendix A. Supplementary data

Supplementary data related to this article can be found at http://dx.doi.org/10.1016/j.jsg.2017.11.011.

## References

Aigner, T., Schauer, M., Junghans, W.D., Reinhardt, L., 1995. Outcrop gamma-ray logging and its applications: examples from the German Triassic. Sediment. Geol. 100 (1–4), 47–61.
Amilibia, A., Sàbat, F., McClay, K.R., Muñoz, J.A., Roca, E., Chong, G., 2008. The role of inherited tectono-sedimentary architecture in the development of the central Andean mountain belt: insights from the Cordillera de Domeyko. J. Struct. Geol. 30 (12), 1520–1539.
Bastida, F., Aller, J., Toimil, N.C., Lisle, R.J., Bobillo-Ares, N.C., 2007. Some considerations on the kinematics of chevron folds. J. Struct. Geol. 29 (7), 1185–1200.
Bistacchi, A., Balsamo, F., Storti, F., Mozafari, M., Swennen, R., Solum, J., Tueckmantel, C., Taberner, C., 2015. Photogrammetric digital outcrop reconstruction, visualization with textured surfaces, and three-dimensional structural analysis and modeling: innovative methodologies applied to fault-related dolomitization (Vajont Limestone, Southern Alps, Italy). Geosphere 11, 2031–2048.
Bluck, B.J., Kelling, G., 1963. Channels from the upper carboniferous coal measures of South Wales. Sedimentology 2 (1), 29–53.
Butler, R.W.H., 1992. Evolution of Alpine fold-thrust complexes: a linked kinematic approach. In: Mitra, S., Fisher, G.W. (Eds.), Structural Geology of Fold and Thrust Belts. John Hopkins University Press, Baltimore, pp. 29–44.
Butler, R.W.H., McCaffrey, W.D., 2004. Nature of thrust zones in deep water sand-shale sequences: outcrop examples from the Champsaur sandstones of SE France. Mar. Pet. Geol. 21 (7), 911–921.
Cawood, A.J., Bond, C.E., Howell, J.A., Butler, R.W., Totake, Y., 2017. LiDAR, UAV or compass-clinometer? Accuracy, coverage and the effects on structural models. J. Struct. Geol. 98, 67–82.
Corbett, K., Friedman, M., Spang, J., 1987. Fracture development and mechanical stratigraphy of Austin Chalk, Texas. AAPG Bull. 71 (1), 17–28.
Couples, G.D., Lewis, H., 1999. Effects of interlayer slip in model forced folds. Geol. Soc. Lond. Spec. Publ. 169 (1), 129–144.
Couzens, B.A., Wiltschko, D.V., 1996. The control of mechanical stratigraphy on the formation of triangle zones. Bull. Can. Pet. Geol. 44 (2), 165–179.
Coward, M.P., Smallwood, S., 1984. An interpretation of the Variscan tectonics of SW Britain. Special Publ. Geol. Soc. 14 (1), 89–102.
Currie, J.B., Patnode, H.W., Trump, R.P., 1962. Development of folds in sedimentary strata. Geol. Soc. Am. Bull. 73 (6), 655–673.
De la Beche, H.T., 1826. On the geology of southern Pembrokeshire. Trans. Geol. Soc. Lond. 2 (1), 1–20.
Dixon, E.E.L., 1933. Notes on the geological succession in south Pembrokeshire. Proc. Geol. Assoc. 44 (4), 402–411.
Druguet, E., Alsop, G.I., Carreras, J., 2009. Coeval brittle and ductile structures associated with extreme deformation partitioning in a multilayer sequence. J. Struct. Geol. 31 (5), 498–511.
Dunne, W.M., 1983. Tectonic evolution of SW Wales during the upper Palaeozoic. J. Geol. Soc. 140 (2), 257–265.
Dunne, W.M., North, C.P., 1990. Orthogonal fracture systems at the limits of thrusting: an example from southwestern Wales. J. Struct. Geol. 12 (2), 207–215.
Farzipour-Saein, A., Yassaghi, A., Sherkati, S., Koyi, H., 2009. Mechanical stratigraphy and folding style of the Lurestan region in the Zagros Fold–Thrust belt, Iran. J. Geol. Soc. 166 (6), 1101–1115.
Ferrill, D.A., Morris, A.P., Smart, K.J., 2007. Stratigraphic control on extensional fault propagation folding: big Brushy Canyon monocline, Sierra del Carmen, Texas. Geol. Soc. Lond. Spec. Publ. 292 (1), 203–217.
Ferrill, D.A., Morris, A.P., 2008. Fault zone deformation controlled by carbonate mechanical stratigraphy, Balcones fault system. Tex. AAPG Bull. 92 (3), 359–380.
Ferrill, D.A., Morris, A.P., McGinnis, R.N., Smart, K.J., Wigginton, S.S., Hill, N.J., 2016. Mechanical stratigraphy and normal faulting. J. Struct. Geol. 94, 275–302.
Fischer, M.P., Jackson, P.B., 1999. Stratigraphic controls on deformation patterns in fault-related folds: a detachment fold example from the Sierra Madre Oriental, northeast Mexico. J. Struct. Geol. 21 (6), 613–633.
Frodsham, K., Gayer, R.A., 1997. Variscan compressional structures within the main productive coal-bearing strata of South Wales. J. Geol. Soc. 154 (2), 195–208.
Gayer, R.A., Jones, J., 1989. The Variscan foreland in South Wales. Proc. Ussher Soc. 7 (2), 177–179.
George, G.T., 1982. Sedimentology of the upper sandstone group (namurian G1) in south-west Dyfed: a case study. In: Bassett, M.G. (Ed.), Geological Excursions in Dyfed, South-west Wales. National Museum of Wales, Cardiff, pp. 203–214 1982.
George, G.T., 2000. Characterisation and high resolution sequence stratigraphy of storm-dominated braid delta and shoreface sequences from the Basal Grit Group (Namurian) of the South Wales Variscan peripheral foreland basin. Mar. Pet. Geol. 17 (4), 445–475.
George, G.T., 2008. The geology of South Wales: a field guide. GT George.
Hancock, P.L., 1973. Structural zones in Variscan Pembrokeshire. Proc. Ussher Soc. 2, 509–520.
Hancock, P.L., Dunne, W.M., Tringham, M.E., 1982. Variscan structures in southwest Dyfed. In: Bassett, M.G. (Ed.), Geological Excursions in Dyfed, South-west Wales. National Museum of Wales, Cardiff, pp. 215–248 1982.
Hayes, M., Hanks, C.L., 2008. Evolving mechanical stratigraphy during detachment folding. J. Struct. Geol. 30 (5), 548–564.
Higgins, S., Clarke, B., Davies, R.J., Cartwright, J., 2009. Internal geometry and growth history of a thrust-related anticline in a deep water fold belt. J. Struct. Geol. 31 (12), 1597–1611.
Hooker, J.N., Laubach, S.E., Marrett, R., 2013. Fracture-aperture size—frequency, spatial distribution, and growth processes in strata-bounded and non-strata-bounded fractures, Cambrian Mesón Group, NW Argentina. J. Struct. Geol. 54, 54–71.
Jenkins, T.B.H., 1962. The sequence and correlation of the coal measures of Pembrokeshire. Q. J. Geol. Soc. 118 (1–4), 65–101.
Kristensen, M.B., Childs, C.J., Korstgård, J.A., 2008. The 3D geometry of small-scale relay

zones between normal faults in soft sediments. J. Struct. Geol. 30 (2), 257–272.
Ladeira, F.L., Price, N.J., 1981. Relationship between fracture spacing and bed thickness. J. Struct. Geol. 3 (2), 179–183.
Laubach, S.E., Olson, J.E., Gross, M.R., 2009. Mechanical and fracture stratigraphy. AAPG Bull. 93 (11), 1413–1426.
Leveridge, B., Hartley, A.J., 2006. The Variscan Orogeny: the development and deformation of Devonian/carboniferous basins in SW England and South Wales. In: Brenchley, P.J., Rawson, P.F. (Eds.), The Geology of England and Wales. Geological Society of London, London, pp. 225–255.
Lloyd, G.E., Chinnery, N., 2002. The Bude Formation, SW England—a three-dimensional, intra-formational Variscan imbricate stack? J. Struct. Geol. 24 (8), 1259–1280.
Mansfield, C.S., Cartwright, J.A., 1996. High resolution fault displacement mapping from three-dimensional seismic data: evidence for dip linkage during fault growth. J. Struct. Geol. 18 (2–3), 249–263.
Martín, S., Uzkeda, H., Poblet, J., Bulnes, M., Rubio, R., 2013. Construction of accurate geological cross-sections along trenches, cliffs and mountain slopes using photogrammetry. Comput. Geosci. 51, 90–100.
Miall, A.D., 1985. Architectural-element analysis: a new method of facies analysis applied to fluvial deposits. Earth Sci. Rev. 22 (4), 261–308.
Mitra, S., 2003. A unified kinematic model for the evolution of detachment folds. J. Struct. Geol. 25 (10), 1659–1673.
Morris, A.P., Ferrill, D.A., McGinnis, R.N., 2009. Mechanical stratigraphy and faulting in Cretaceous carbonates. AAPG Bull. 93 (11), 1459–1470.
Nicol, A., Gillespie, P.A., Childs, C., Walsh, J.J., 2002. Relay zones between mesoscopic thrust faults in layered sedimentary sequences. J. Struct. Geol. 24 (4), 709–727.
Pfiffner, O.A., 1985. Displacements along thrust faults. Eclog. Geol. Helv. 78, 313–333.
Pfiffner, O.A., 1993. The structure of the Helvetic nappes and its relation to the mechanical stratigraphy. J. Struct. Geol. 15 (3–5), 511–521.
Poblet, J., Lisle, R.J., 2011. Kinematic evolution and structural styles of fold-and-thrust belts. Geol. Soc. Lond. Spec. Publ. 349 (1), 1–24.
Powell, C.M., 1989. Structural controls on Palaeozoic basin evolution and inversion in southwest Wales. J. Geol. Soc. 146 (3), 439–446.
Ramsay, J.G., 1974. Development of chevron folds. Geol. Soc. Am. Bull. 85 (11), 1741–1754.
Rarity, F., Van Lanen, X.M.T., Hodgetts, D., Gawthorpe, R.L., Wilson, P., Fabuel-Perez, I., Redfern, J., 2014. LiDAR-based digital outcrops for sedimentological analysis: workflows and techniques. Geolo. Soc. Lon. Spec. Publ. 387 (1), 153–183.
Roche, V., Homberg, C., Rocher, M., 2012. Architecture and growth of normal fault zones in multilayer systems: a 3D field analysis in the South-Eastern Basin, France. J. Struct. Geol. 37, 19–35.
Smallwood, S., 1985. A thin-skinned thrust model for Variscan Pembrokeshire, Wales. J. Struct. Geol. 7 (6), 683–687.
Tavani, S., Storti, F., Salvini, F., Toscano, C., 2008. Stratigraphic versus structural control on the deformation pattern associated with the evolution of the Mt. Catria anticline, Italy. J. Struct. Geol. 30 (5), 664–681.
Totake, Y., Butler, R.W., Bond, C.E., Aziz, A., 2017. Analyzing structural variations along strike in a deep-water thrust belt. J. Struct. Geol (In Press), Available online 14 June 2017.
Tringham, M.E., 1985. Tectonic deformation of a channel sandstone. Geol. J. 20 (3), 247–255.
Van Noorden, M., Sintubin, M., Darboux, J.R., 2007. Incipient strain partitioning in a slate belt: evidence from the early Variscan Monts d'Arrée slate belt (Brittany, France). J. Struct. Geol. 29 (5), 837–849.
Vergés, J., Goodarzi, M.G.H., Emami, H., Karpuz, R., Efstathiou, J., Gillespie, P., 2011. Multiple detachment folding in Pusht-e Kuh arc, Zagros: role of mechanical stratigraphy. In: In: McClay, K., Shaw, J., Suppe, J. (Eds.), Thrust Fault-related Folding: AAPG Memoir, vol. 94. pp. 69–94.
Waters, C.N., Waters, R.A., Barclay, W.J., Davies, J.R., 2009. A Lithostratigraphical Framework for the Carboniferous Successions of Southern Great Britain (Onshore). British Geological Survey Research Report, RR/09/0.
Williams, P.F., 1968. The sedimentation of Westphalian (Ammanian) measures in the little Haven-Amroth Coalfield, Pembrokeshire. J. Sediment. Petrol. 38 (2), 332–362.
Willis, B., 1893. The Mechanics of Appalachian Structure. U.S. Geological Survey, pp. 211–281 13th Annual Report, pt. 2.
Woodward, N.B., Rutherford, E., 1989. Structural lithic units in external orogenic zones. Tectonophysics 158 (1–4), 247–267.
Zahm, C.K., Hennings, P.H., 2009. Complex fracture development related to stratigraphic architecture: challenges for structural deformation prediction, Tensleep Sandstone at the Alcova anticline. Wyo. AAPG Bull. 93 (11), 1427–1446.